IEEE Access
Multidisciplinary | Rapid Review | Open Access Journal

Received 24 June 2022, accepted 20 July 2022, date of publication 1 August 2022, date of current version 12 August 2022.

Digital Object Identifier 10.1109/ACCESS.2022.3195936

RESEARCH ARTICLE

A Novel High Gain Dual Input Single Output Z-Quasi Resonant (ZQR) DC/DC Converter for Off-Board EV Charging

S. HARINI[1], N. CHELLAMMAL[1], (Member, IEEE), BHARATIRAJA CHOKKALINGAM[1], (Senior Member, IEEE), AND LUCIAN MIHET-POPA[2], (Senior Member, IEEE)

[1]Department of Electrical and Electronics Engineering, SRM Institute of Science and Technology, Chennai 603203, India
[2]Department of Electrical Engineering, Faculty of Engineering, Østfold University College, 1757 Halden, Norway

Corresponding authors: N. Chellammal (chellavenkat09@gmail.com) and Lucian Mihet-Popa (lucian.mihet@hiof.no)

This work was supported in part by the Department of Science and Technology, Government of India, through the Promotion of University Research and Scientific Excellence (PURSE) under Award SR/PURSE/2021/65.

ABSTRACT This manuscript focuses on a multi-port non-isolated (Dual input and single output) DC/DC power electronic interface based on Z-Quasi Resonant (ZQR) network. The converter accommodates grid and Photovoltaic panel (PV) as its input sources. Unlike the basic DC/DC converters, the recommended DC/DC converter requires fewer switches and provides continuous current, high gain in voltage, and minimal voltage stress on converter switch up to 40% duty cycle owing to the presence of ZQR network. This feature of the converter makes it to find its application in Electric Vehicle (EV) off-board charging where high voltage gain is required. In the proposed multi-port ZQR converter, additional input and output ports could be appended without compromising the converter's gain and efficiency. The developed converter can operate continuously even if any one of the input sources fails to charge the EV. The proposed converter is mathematically modeled using basic laws that govern the converter performance and analyzed in MATLAB simulink platform under various operating modes. A detailed analysis under steady-state, dynamic conditions and a comparison of the developed multiport ZQR DC/DC converter with the topologies addressed in published literature are also presented in this manuscript. In order to verify the proposed converter performance, a prototype model of 300 W has been fabricated with switching frequency of 20 kHz. Experimental results confirm the effectiveness of the theoretical analysis, the aforementioned advantages, and features of the proposed multiport ZQR DC/DC converter.

INDEX TERMS Multi-port, quasi-resonant, DC/DC converter, photovoltaic, battery, electric vehicle, charging.

I. INTRODUCTION

Aggregating environmental pollution due to greenhouse gas emission, rapid rise in fuel cost, and depletion of fossil fuels are justifiable reasons for the development of electric vehicular technologies. Therefore, automobile industries have started manufacturing EVs with clean and renewable energy sources instead of fossil-fuel vehicles. As the deployment of EV increases, the charging infrastructure which play a crucial role needs more attention on research and development On an average, Indian car owners drive about 35 km/day-a range, the newly developing EVs can meet in a single charge. Though positive evidence on EVs has become very clear, one of the main hurdles to EV are driving range concern and charging infrastructure. The driving range can be improved with proper control of batteries. Conversely, in order to overcome the charging time anxiety, chargers capable of reducing the charging time and complying with grid standards should be developed. Over the past few years, high-gain DC/DC converters have attracted special attention

The associate editor coordinating the review of this manuscript and approving it for publication was Amin Hajizadeh.

This work is licensed under a Creative Commons Attribution 4.0 License. For more information, see https://creativecommons.org/licenses/by/4.0/

in several application areas, especially in hybrid renewable energy systems, EV charging, and grid integrated PV systems where the generated voltage levels of the battery and the PV panel are typically low and require a voltage lift. In such applications, utilization of high gain converters is essential. On the primary side, a full or half-bridge current source circuit is proposed, with a quasi-switched capacitor circuit on the secondary side for dual-input bidirectional DC/DC converters in [1]. A comparative evaluation of various power electronic topologies of the converter appropriate for EV with a battery, EV with a plug-in hybrid powertrain, and EV rapid charging have been reviewed in [2]. A thorough examination of advancement needed in isolated and non-isolated power electronic topologies for EV charging along with soft switching auxiliary circuits have been carried out in [3]. Two types of DC/DC converters are available: one is isolated [4], [5] and another is non-isolated [6], [7]. For safety concerns, some applications require isolation. Transformers achieve a high gain in voltages and in isolated converters, focus on providing electrical isolation between input and output. The voltage/power gain can be easily improved with these sorts of converters by raising the transformer turn ratio [8]. The performance of such isolated converters can be degraded by a huge proportion of components, significant energy losses, and possibilities of transformer saturation. However, if isolation is not essential, a non-isolated power DC/DC converter comprising of a transformer-less single circuit transfers power among the input and output. Such conventional transformer-less converters are simpler, cost/space effective, and more efficient than isolated circuits owing to the absence of transformer saturation. However, they deliver low voltage gain. Many architectures and different methodologies have been implemented in the literature to compensate for transformer-less DC/DC converters with lower voltage gain. Switched inductor [9], [10], switched capacitor [11], topologies in cascaded [12], lift-voltage [13], switched boost [14], and multiply cells [15] are some widely used methodologies to enhance the voltage gain of the converters. Although, combining these approaches can further improve the converter's voltage gain, the complexity, and expenditure eventually rise. The high gain in voltage and efficiency of converters [16]–[18] are achieved with the control of the coupling inductor. A bidirectional non-isolated zero voltage transition converter for charging and discharging energy storage devices is proposed in [19]. Basic idea of boost DC/DC power converters with the enhancements to modify the structure is proposed in [20]. The study is primarily concerned with the selection of model expression in order to avoid problems associated with state matrices singularity. The converter with continuous incoming current and low output current ripple capable of providing current transfer between two interleaved modules without the use of an additional current-sharing control method is presented in [21]. Though interleaved boost converter (IBC) and Full-Bridge converter (FBC) have the ability to provide high efficiency of roughly 92% at full load, however, there exist switching losses in IBC [22] and the dimension of FBC [23] rises owing to the employment of transformer with a high frequency in conjunction with the inductor. It is indispensable to suppress electromagnetic interference in both the converters. Various recharging methods mainly applicable for off-board (direct-current) fast charging along with the genetic algorithm to estimate the optimal charging system size are presented in [24]. A comprehensive survey of future perspectives of EVs based on infrastructures for recharging PHEV/PEV batteries, energy management, vehicle-to-grid (V2G), and requirement of collaboration, importance of industrial information technologies are discussed in [25]. Driving range issues and charging infrastructure are the most significant barriers to EV adoption. Chargers are divided into three categories based on the power rating of EV batteries: level-1, level-2, and level-3 [26]. Normally, AC level-1 or level-2 home chargers are suitable for nocturnal charging in downtown areas, but not for long-distance travel. To overcome these obstacles, appropriate off-board (level 3/DC off-board) charging stations with quick battery charging and high output gain must be developed. A DC/DC boost converter with high-gain in voltage, such as ZQR DC/DC converter based on soft switching (ZQR) converter is of good choice. But the converter proposed in [27] is a single input single output converter. A Z-source converter employing a unique impedance network suitable for AC/DC, DC/DC, DC/AC, AC/AC power conversion is suggested in [28]. The implementation of a three-level LLC converter topology based on Si-FETs with reduced voltage strain on the switches is discussed [29]. A reconfigured topology of the step-up DC/DC converter with sources in parallel and output in series using two quasi z source networks is developed to enhance the voltage gain and decrease the voltage stress across the power semiconductors [30]. The ZQR converter network offers several significant features, including constant input current, minimal capacitor voltage stress, and common ground linking the input and output of the circuit. Because of these benefits, this impedance network is ideal for a wide range of applications. The converters [31]–[33] employ a huge proportion of components, and some have a limited potential for improvement. For example, efficiency is a measure to select DC/DC converters for every application. It should be greater than 75% for a typical DC/DC boost converter. But, in such converters, the necessary output voltage is achieved only above 0.5 duty cycle. A typical DC/DC boost converter's efficiency is approximately 60% at 0.8 duty cycle, which is unsuitable for EV applications. ZQR DC/DC converter, which increases the booster capacity in the low service cycles, reduces voltage stress across the switch. In general, in ZQR DC/DC converter, the desired output voltage and efficiency above 75% can be achieved even below 0.5 duty cycle.

In addition, the need and systematic way of deriving multiport converter based on dc-link inductor (DLI) concept are presented in [34], [35]. As mentioned in the above literature, the impediments related to the DC/DC converter

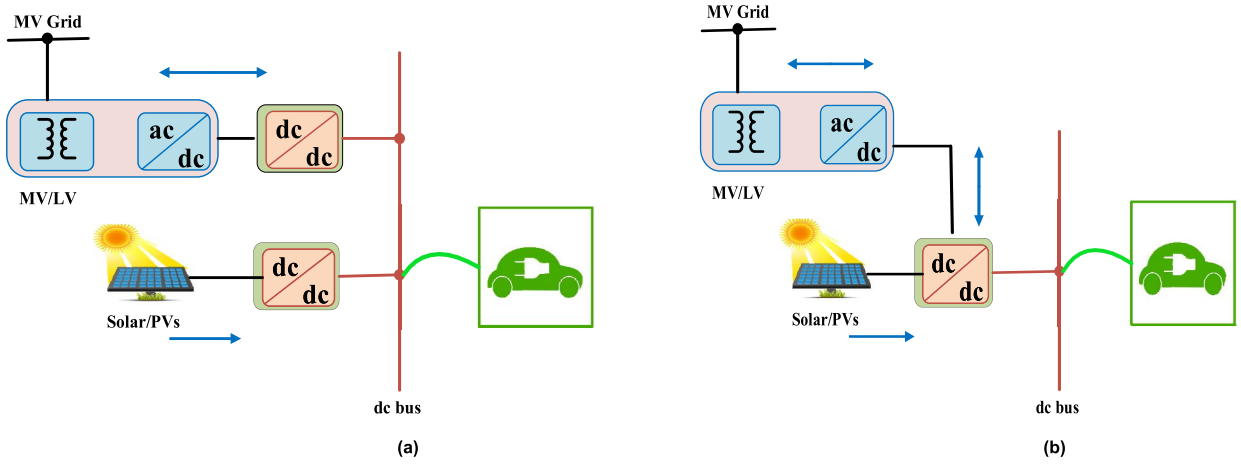

FIGURE 1. Block diagram of (a) Conventional (b) Proposed three port ZQR converter in an EV charging system.

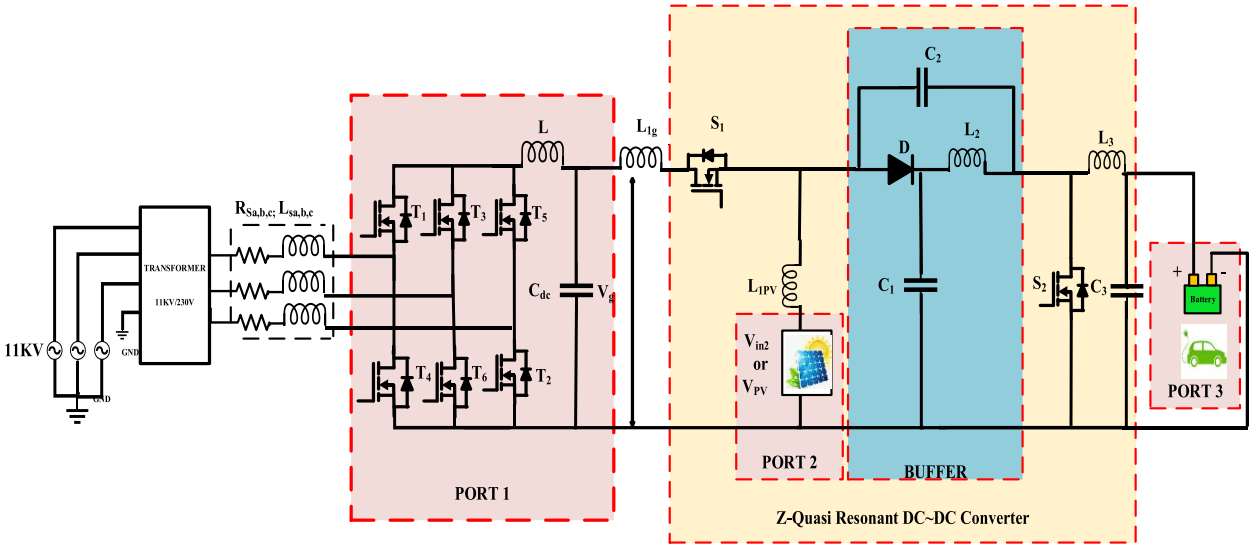

FIGURE 2. Proposed non-isolated multi-port ZQR DC/DC converter for EV off-board charging system configuration.

used for fast charging, encourage to probe about the new DC/DC converters at low switch voltage stress, reduced charging time, high efficiency, and increased voltage gain. To address these issues, a ZQR converter using a resonant tank as buffer interface fed with multiple power sources is proposed in this paper. The power contribution from PV and grid is increasing to improve the quality and quantity of the power delivered. A hybrid energy system, which combines diverse renewable energy sources with varying voltage/current characteristics, is essential. As shown in Figure 3, the proposed three-port non-isolated ZQR DC/DC converter has one PV port, a rectified output from the grid port, and an output port. The feature of the converter thus presented opens a new horizon in the sector of EV battery fast charging. With this intention, the working principle, and mathematical derivation of gaining steady-state performance are documented in Section II. The considerations in design and the efficiency calculation along with loss analysis are presented in Sections III and IV respectively. To elucidate the features, the proposed converter topology is compared to

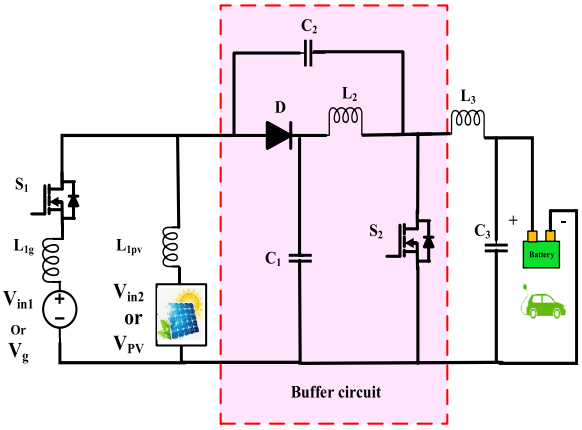

FIGURE 3. Proposed three port ZQR DC/DC converter.

various converters that have been published in the literature in Section V. A prototype of the proposed converter is realized, and the results of the experiments are presented in Section VI to validate the simulated and theoretical analyses. In Section VII, the dynamic behavior of the converter is

TABLE 1. Operating modes of proposed multiport ZQR DC/DC converter.

Mode	Input	Output	Energy flow direction	Type of Mode
Mode-1	Port-1	Port-3	Grid to EV battery Figure 5 (a)	Single Input Single Output (SISO)
Mode-2	Port-2	Port-3	PV to EV battery Figure 5 (b)	Single Input Single Output (SISO)
Mode-3	Port -1 and Port-2	Port-3	Grid and PV to EV battery Figure 5 (c)	Dual Input Single Output (DISO)

presented. Finally, the findings drawn are concluded in Section VIII.

II. SCHEMATIC AND OPERATION MODES OF PROPOSED CONVERTER

Due to the widespread use of electric cars, a single source of energy will be insufficient to satisfy the load demand. Consequently, various energy sources need to be combined. This paper aims to synthesize a topology converter that can couple different power sources to EV batteries. Figures 1 (a) and (b) indicate the power electronic interface's significance in the power system of an EV. Figure 2 shows the configuration of the proposed multiport ZQR converter. The following are some of the proposed multiport ZQR DC/DC converter's most notable features:

- Individual energy glide manipulates among the sources.
- Easy design, manipulation, and implementation process.
- Higher gain at a low duty cycle.

In the Figure 3 shows the designed triple port ZQR DC/DC converter's power circuit. This circuit consists of two power-controlled switches (S_1 and S_2), three capacitors (C_1, C_2, and C_3), and four inductors (L_{1g}, L_{1pv}, L_2, and L_3), one uncontrolled switch D, and EV battery. The power switches S_1 and S_2 are controlled switches to transfer the energy from grid (Port 1) and PV (Port 2) to EV battery (Port 3). Thus, grid and photovoltaic panel are connected as input ports at port1 and port 2 respectively and the EV battery is connected as an output port at port 3. According to the availability of input sources and according to the switching states of switches S_1, S_2, the proposed three-port converter has three modes and two distinct states in each operating mode. Figures 4 and 5 show the various modes of operation and the equivalent circuits of the proposed converter for each interval of the operating period. The fundamental waveforms of the suggested converter shown in Figure 6 are related to pulses of switches S_1, S_2, currents of L_{1g}, L_{1pv}, L_2, L_3, and voltages of C_1, C_2. Table 1 provides information about the ports involved and the direction of the power flow in the proposed multiport ZQR DC/DC converter during different operating modes. For simplification of analysis, the switches, diodes, inductors, and capacitors are considered to be ideal.

A. MODE 1 SISO [SINGLE INPUT SINGLE OUTPUT] ($V_g > V_{PV}$)

The equivalent circuit and the power flow schematic of the proposed converter for mode-1 operation are shown in Figure 5 (a). In this condition, the grid transfers power to the EV battery individually. Table 2 displays the switching procedures of individual operating devices.

1) STATE 1

During this period $0 < T < d_1T$, the switches S_1 and S_2 are turned on as shown in Figure 5 (a) (i). The current I_{L1g} flowing through the inductor L_{1g} rises with a positive slope. Capacitor C_2 discharges to magnetize the L_2 inductor and charge the capacitor C_1. As a consequence inductor L_3, and capacitor C_2 are discharging. It can be seen from Figure 6 (a) that the drive pulses for S_1 and S_2 remain the same for State 1. The equations (1) to (5) are valid for state 1 operation.

$$V_g = V_{L1g} - V_{C2} \tag{1}$$
$$V_{L1g} = V_g + V_{C2} \tag{2}$$
$$V_{L2} = V_{C1} \tag{3}$$
$$V_{L3} = -V_{C3} \tag{4}$$
$$V_{C3} = V_O \tag{5}$$

2) STATE 2

During this period $d_1T < T < T$, as shown in Figure 5 (a) (ii), the enabling switch S_1 and turning off of switch S_2 result in the drop of inductor current i_{L1g} with a negative slope. Inductor L_2 and capacitor C_1 are discharging. L_3 and C_2 are charging. The steady state equations corresponding to the state are elucidated as shown in equation (6) to (10).

$$V_g = V_{L1g} + V_{C1} \tag{6}$$
$$V_{L1g} = V_g - V_{C1} \tag{7}$$
$$V_{L2} = -V_{C2} \tag{8}$$
$$V_{C1} - V_{L2} - V_{L3} - V_{C3} = 0 \tag{9}$$
$$V_{C3} = V_{C1} - V_{L2} - V_{L3} \tag{10}$$

The switching period terminates at the end of state 2. The equivalent circuit of the proposed ZQR DC/DC converter operating in this mode is shown in Figure 5 (a). The voltages across the capacitor and the gain in voltage can be extracted as mentioned in equation (11-14) by considering the volt-second balance equation (1-10) of the inductor and charge second balance of the capacitor

$$V_{C1} = \frac{(1-d_1)\,V_{in1}}{(1-2d_1)} \tag{11}$$
$$V_{C2} = \frac{d_1 V_{in1}}{(1-2d_1)} \tag{12}$$

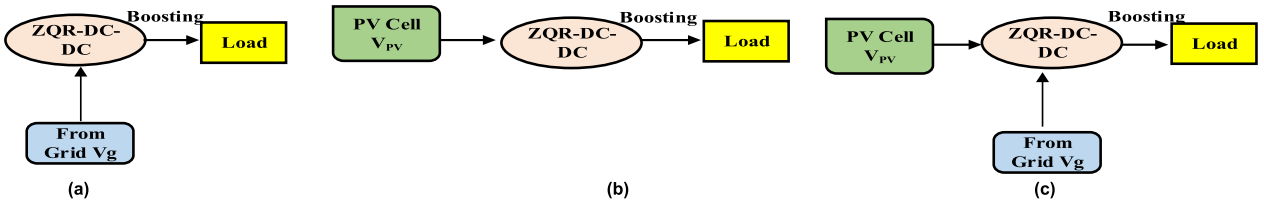

FIGURE 4. (a) MODE 1 (From grid (V_g) to EV battery (Load); (b) MODE 2 (From PV (V_{dc}) to EV battery (Load); (c) MODE 3 (From grid (V_g) and PV (V_{dc}) to EV battery (Load).

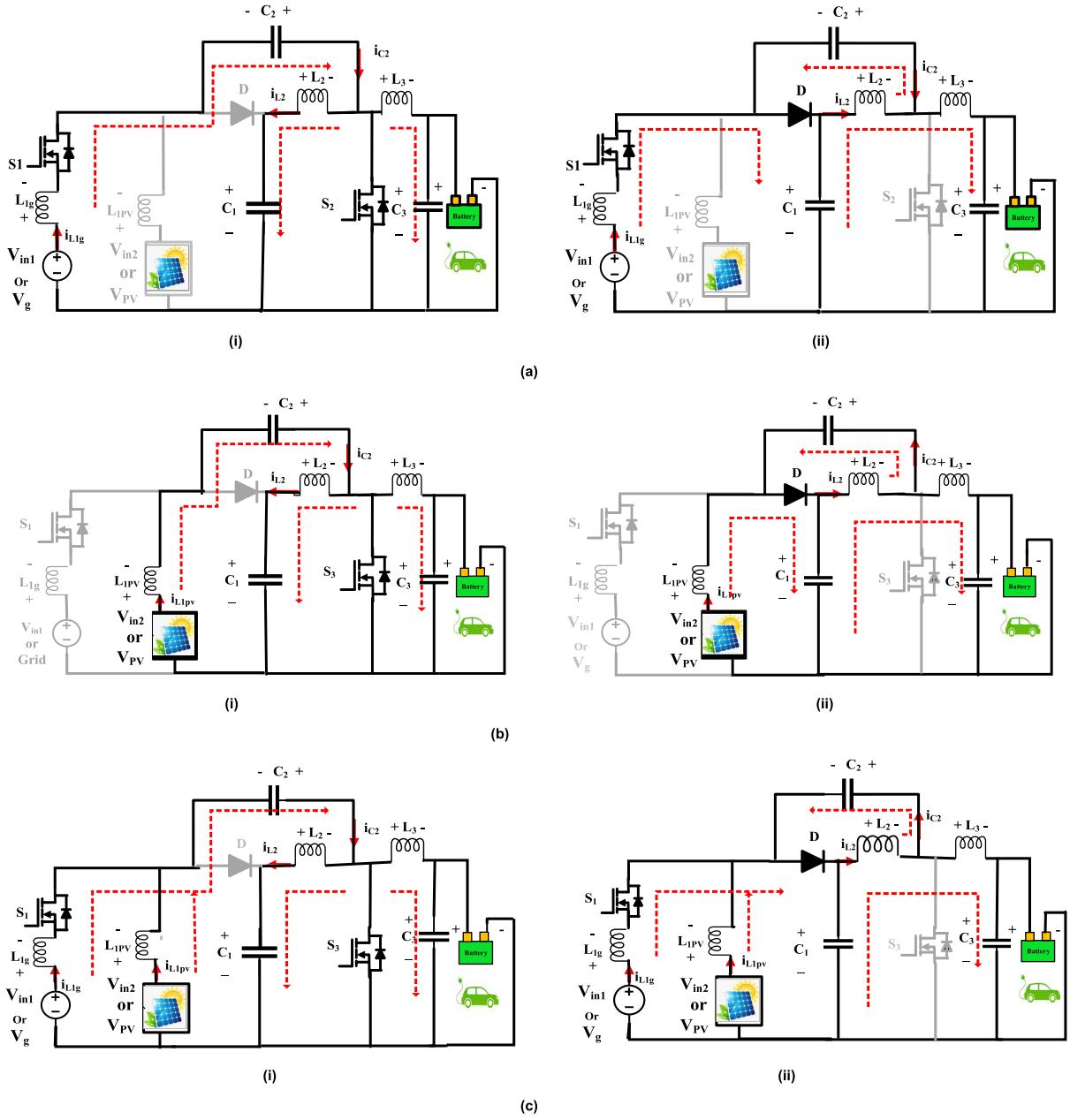

FIGURE 5. Equivalent circuits of proposed converter (a) Mode 1 From grid (V_g) to EV battery (Load) (b) Mode 2 From PV (V_P) to EV battery (Load) (c) Mode-3 From grid (V_g) & PV (V_{PV}) to EV battery (Load).

$$V_{o1} = \frac{(1-d_1)\,V_{in1}}{(1-2d_1)} \tag{13}$$

$$V_{bat} = \frac{(1-d_1)\,V_g}{(1-2d_1)} \tag{14}$$

B. MODE 2 SISO [SINGLE INPUT SINGLE OUTPUT] - ($V_{PV} > V_G$)

In this condition, the PV transfers energy to the EV battery in this mode individually

TABLE 2. State of operation.

Mode	Input Source	MOSFET Switches		Inductors			Diode	Capacitors		Battery	Output Voltage
		S_1	S_2	L_{1g}	L_{1PV}	L_2	D	C_1	C_2	V_{bat}	V_O
Mode 1 ($V_g > V_{PV}$)	V_g	ON	ON	↑	-	↑	OFF	↑	↓	Charging	Boost
		ON	OFF	↓	-	↓	ON	↓	↑	Charging	Boost
Mode 2 ($V_g < V_{PV}$)	V_{PV}	OFF	ON	-	↑	↑	OFF	↑	↓	Charging	Boost
		OFF	OFF	-	↓	↓	ON	↓	↑	Charging	Boost
Mode 3 ($V_g = V_{PV}$)	V_g and V_{PV}	ON	ON	↑	↑	↑	OFF	↑	↓	Charging	Boost
		ON	OFF	↓	↓	↓	ON	↓	↑	Charging	Boost

Table representation : ON-Switch close; OFF-Switch open ↑Charging of inductor and capacitor; ↓ Discharging of inductor and capacitor.

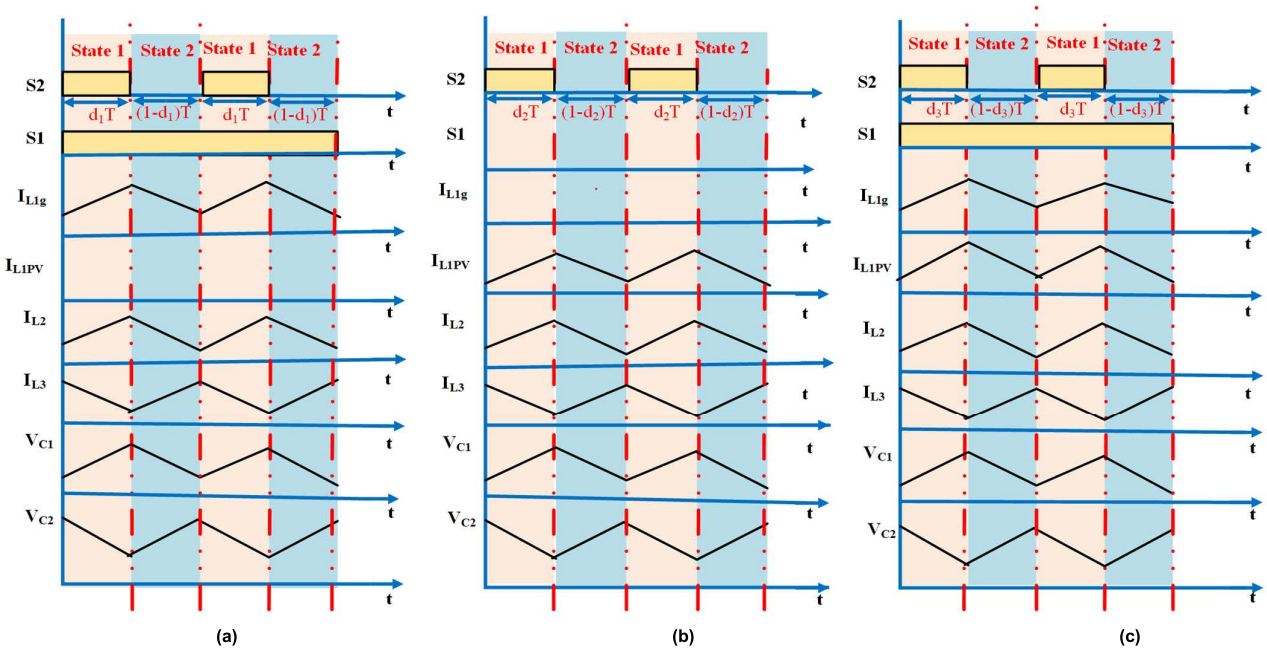

FIGURE 6. Characteristic waveforms of proposed converter (a) Mode 1 (From grid (V_g) to EV battery (Load) (b) Mode 2 (From PV (V_{PV}) to EV battery (Load) (c) Mode-3 (From grid (V_g) & PV (V_{PV}) to EV battery Load).

1) STATE 1

During this period $0 < T < d_2T$, the switches S_2 is turned on and S_1 are switched off as shown in Figure 5 (b) (i), The voltage V_{PV}, causes the rise in inductor current I_{L1PV} with a positive slope. Capacitor C_2 discharges to magnetize the L_2 and charge the capacitor C_1. Inductor L_3 and capacitor C_2 start discharging.

$$V_{In2} = V_{L1pv} - V_{C2} \tag{15}$$
$$V_{L1pv} = V_{In2} + V_{C2} \tag{16}$$
$$V_{L2} = V_{C1} \tag{17}$$
$$V_{L3} = -V_{C3} \tag{18}$$
$$V_{C3} = V_O \tag{19}$$

2) STATE 2

During this period $d_2T < T < T$ as shown in Figure 5 (b) (ii), S_1 and S_2 are turned off. The L_{1PV} is inductive, resulting in the drop of the inductor current with a positive slope. Inductor L_2 and capacitor C_1 start discharging. Inductor L_3 and capacitor C_2 are charging

$$V_{In2} = V_{L1pv} + V_{C1} \tag{20}$$
$$V_{L1pv} = V_{In2} - V_{C1} \tag{21}$$
$$V_{L2} = -V_{C2} \tag{22}$$
$$V_{C1} - V_{L2} - V_{L3} - V_{C3} = 0 \tag{23}$$
$$V_{C3} = V_{C1} - V_{L2} - V_{L3} \tag{24}$$

The switching period ends when the second state ends. The Figure 6 (b) shows the characteristic waveforms of the proposed multiport ZQR DC/DC converter in mode 2. It can be seen from Figure 6 (b) that the drive pulses from S_1 and S_2 are the same. The capacitors voltages and the voltage gain equation can be obtained as mentioned in equations (25-28) concerning the volt-second balance equations (15-24) of the

inductors and capacitors.

$$V_{C1} = \frac{(1-d_2)\,V_{in2}}{(1-2d_2)} \tag{25}$$

$$V_{C2} = \frac{d_2 V_{in2}}{(1-2d_2)} \tag{26}$$

$$V_{02} = \frac{(1-d_2)\,V_{in2}}{(1-2d_2)} \tag{27}$$

$$V_{bat} = \frac{(1-d_2)\,V_{PV}}{(1-2d_2)} \tag{28}$$

C. MODE 3 DISO [DUAL INPUT SINGLE OUTPUT] POWER TRANSFER FROM GRID (V_g) AND PV (V_{PV}) TO EV BATTERY (LOAD)

When EV battery demand is high, the Grid and PV together provide the sufficient power to meet the demand. In this condition, both PV and grid supply energy to EV battery. During this state, switch S_1 is turned on.

1) STATE 1

During this period $0 < T < d_3T$ as shown in Figure 6 c, the switches S_1 and S_2 are turned on and the state equivalent circuit of the converter during this operation is displayed in Figure 5 c(i). The voltage V_g and V_{PV}, cause a rise of inductor current I_{L1g} and I_{L1PV} respectively with a positive slope. Inductor L_2 and capacitor C_1 are charging. Inductor L_3 and capacitor C_2 are discharging.

$$I_{L1g} + I_{L1pv} = I_{C2} \tag{29}$$

$$I_{L2} + I_{L3} = I_{C2} \tag{30}$$

$$I_{L2} = I_{C1} \tag{31}$$

$$I_{L3} = I_0 + I_{C3} \tag{32}$$

$$I_{C3} = I_{L3} - I_0 \tag{33}$$

2) STATE 2

During this period $d_3Ts < T < T$, the switch S_1 is enabled and S_2 is turned off as shown in Figure 5 c(ii). Inductor L_{1g} and L_{1PV} are inductive, resulting in the drop of inductor current with a negative slope. Inductor L_2 and capacitor C_1 discharging. L_3 and C_2 are charging. The capacitors voltages and the voltage gain equations can be extracted as mentioned in equation (38-41) considering the current-second balance equation (29-37) of the inductors and capacitors.

$$I_{L1g} + I_{L1pv} = I_D + I_{C2} \tag{34}$$

$$I_{C2} = I_{L1g} + I_{L1pv} - I_D \tag{35}$$

$$I_{C1} = I_{L2} - I_D \tag{36}$$

$$I_{C2} = I_{L3} - I_{L2} \tag{37}$$

$$V_{C1} = \frac{(1-d_3)\,(V_g + V_{pv})}{(1-2d_3)} \tag{38}$$

$$V_{C2} = \frac{d_3(V_g + V_{pv})}{(1-2d_3)} \tag{39}$$

$$V_{03} = \frac{(1-d_3)V_{in1}+V_{in2}}{(1-2d_3)} \tag{40}$$

$$V_{03} = \frac{(1-d_3)V_g+V_{pv}}{(1-2d_3)} \tag{41}$$

III. DESIGN OF COMPONENT

A. INDUCTOR

In order to design the inductor, the current ripple of the inductor is required. $V_L = L(di/dt)$ into consideration, the current ripple is expressed as in equation (42)

$$\Delta I_{L1} = \frac{V_{in}\,(1-d)}{(1-2D)\,f_s L_{1g}} \tag{42}$$

The inductors are designed to assure that the peak-to-peak inductor current difference, i_{L1}(peak-peak), does not surpass a maximum of 20% of the average inductor current. Furthermore, the highest feasible input voltage was employed in the computations. Inductors L_{1g} and L_{1PV} are designed as per equation (43) using the required current ripple of the inductor and the inductor volt-sec balancing theory

By solving the equation (1-10), (15-24),inductors L_{1g} and L_{1PV} are designed as in equation (43 & 44).

$$L_{1g} = \frac{R\,(1-2d)}{x_{L1}\%f_s d} \tag{43}$$

where f_s indicates switching frequency.

Similarly, inductor value for L_2 and L_3 are designed as mentioned in equation (44).

$$L_2 \quad or \quad L_3 = \frac{R\,(1-2d)}{x_{L2,3}\%f_s d} \tag{44}$$

B. CAPACITOR

The capacitors are designed to assure that the peak-to-peak capacitor voltage difference, ΔV_C(peak-peak) as derived in equation (45), does not exceed 20% of the average inductor current.

$$\Delta V_{C1} = \frac{V_{in}\,(1-d)\,d}{R\,(1-2d)^2 f_s C_1} \tag{45}$$

Capacitor C_1 is designed as shown in equation (46) using the capacitor voltage charge-sec balance and voltage ripples

$$C_1 = \frac{d}{x_{C1}\%R\,(1-2d)\,f_s D} \tag{46}$$

Similarly, capacitor value for capacitors C_2 and C_3 are designed in equation (47).

$$C_2\ (or)\ C_3 = \frac{d}{x_{C1}\%R\,(1-2d)\,f_s D} \tag{47}$$

IV. EFFICIENCY AND POWER LOSSES ANALYSIS

Parasitic resistances are defined as follows for the efficiency analysis of the proposed multiport ZQR DC/DC Converter: r_s represents switched ON-state resistances, r_D for diode D forward resistance, V_D for diode D threshold voltages, and R_{L1g}, R_{L1PV}, L_2, and L_3 for equivalent series resistance of inductors L_{1g}, L_{1PV}, L_2, and L_3, respectively. The equivalent series resistances of capacitors C_1, C_2, and C_3 are R_{C1}, R_{C2}, and R_{C3}, respectively.

The total power loss of the switch $S_2(P_S)$ can be derived as per equation (48).

$$P_S = P_{rs} + \frac{P_{SL}}{2} \tag{48}$$

The switch S endures from a power conduction loss. (P_{rs}) can be computed using equation(49) & (50)

$$P_{rs} = r_S I_S^2 \tag{49}$$

$$P_{rs} = r_S \left(\frac{dI_O}{(1-2d)} \right)^2 \tag{50}$$

The switching loss of the proposed converter (P_{SL}) can be

$$P_{SL} = f_S C_S \left(\frac{V_{in}}{(1-d)} \right)^2 \tag{51}$$

Substitute (50) & (51) in (48)

$$P_S = 3.15414\text{W} \tag{52}$$

The overall power loss of the Diode D (P_D) can be computed as follows:

$$P_D = P_{FRD} + P_{FVD} \tag{53}$$

The diode D forward resistance loss(P_{FRD}) can be computed as per the equations (54-55).

$$P_{FRD} = r_D I_D^2 \tag{54}$$

$$P_{FRD} = r_D \left(\frac{I_O}{(1-2d)} \right)^2 \tag{55}$$

The diode D forward voltage loss(P_{FVD}) can be computed as follows

$$P_{FVD} = V_D I_D \tag{56}$$

Substitute (55) & (56) in (53)

$$P_D = 1.51\text{ W} \tag{57}$$

The power losses of capacitors C_1, C_2, and C_3 as a result of equivalent series resistance can be obtained using equations (58-62).

$$P_C = P_{RC} \tag{58}$$

$$P_{RC1,2,3} = R_{C1,2,3} I_{C1,2,3}^2 \tag{59}$$

$$P_{RC1,2,3} = R_{C1,2,3} \left(\frac{-dI_O}{(1-2Dd)} \right)^2 \tag{60}$$

$$P_{RC1} = P_{RC2} = P_{RC3} = 1.06\text{ W} \tag{61}$$

$$P_{RC1,2,3} = 3(P_{RC1,2,3}) = 3.18\text{ W} \tag{62}$$

The power losses of inductors L_{1g}, L_{1PV}, L_2, and L_3 as a result of equivalent series resistance can be obtained as follows:

$$P_L = P_{RL} \tag{63}$$

$$P_{RL1,2,3} = R_{L1,2,3} I_{L1,2,3}^2 \tag{64}$$

$$P_{RL1,2,3} = R_{L1,2,3} \left(\frac{(1-d)I_O}{(1-2d)} \right)^2 \tag{65}$$

$$P_{RL1} = P_{RL2} = P_{RL3} = 1.0006 \tag{66}$$

$$P_{RL1,2,3} = 3(P_{RL1,2,3}) = 3.018\text{ W} \tag{67}$$

The total power losses of multiport ZQR DC/DC converter

$$P_{Loss} = P_S + P_D + \sum_{k=1}^{3} P_{RL} + \sum_{k=1}^{3} P_{CL} \tag{68}$$

$$P_{Loss} = 3.15414 + 1.5 + 3.18 + 3.018 \tag{69}$$

$$P_{Loss} = 10.08\text{ W} \tag{70}$$

The efficiency of multiport ZQR DC/DC converter can be defined as:

$$\eta = \frac{P_O}{P_O + P_{Loss}} \tag{71}$$

$$\eta = \frac{1}{1 + \frac{10.08}{94.16}} \tag{72}$$

$$\eta = 91.5\% \tag{73}$$

The power losses in the proposed multiport ZQR DC/DC converter are clearly conduction losses in the inductor cables and capacitors. Winding conduction loss becomes more evident in maximum gain in voltage and output powers, which is due to the matching maximum current flow. As a result, better-graded wires for linked inductors and significantly greater capacitors (with lower ESR) can be employed to improve the proposed multiport ZQR DC/DC converter's conversion efficiency.

V. COMPARISON WITH SIMILAR CONVERTER

Figure 7 illustrates a detailed evaluation of DC/DC converters for off-board EV battery charging. The expense of DC/DC conversions for BEVs is an important factor to consider when developing a charging system. The quantity of switches, transformers, capacitors, diodes, and inductors employed in various DC/DC converts must be used to predict a relative cost. According to this, the calculated cost for conventional boost converter and boost converter with resonant converter is low since both topologies employ a lesser number of components. Because of large component counts and the usage of high frequency transformer or numerous inductors in such converters, the prices are affordable for IBC [19], [20], FBC [23], and ZVSC [2], [5]. Voltage gain is also an important factor to consider when designing the system. Boost converter is unique in that as it requires only a basic control system. The EMI requirements are extremely basic. It is cost-effective because the general circuitry is simple, but the use of higher capacitors increases the volume, making it unsuitable for high-power conversion. At full load, both IBC and FBC have the potential for high efficiency of around 92 percent. Current ripples are minimal, however switching losses exist in IBC, and the volume of FBC increases due to the use of a high-frequency transformer with an inductor. Both converters have the necessity for EMI suppression. Moreover, Table 3 represents the proposed converter has a high gain in voltage, less voltage stress and low cost. Thus, it can be claimed that the proposed multiport ZQR converter is suitable for dc off-board charging EV. The proposed multiport ZQR DC/DC converter synchronized with EV battery is simulated using MATLAB R2015a. To ensure the accuracy of simulation, a 300 W prototype experimental is built.

TABLE 3. Comparison between various DC/DC converters.

	Reference[19,20]	Reference [21]	Reference [2,22]	Reference [2,5]	Proposed Converter
Gain	$\frac{1}{(1-d)}$	$\frac{d}{(2-d)}$	$\frac{2d+1}{(1-d)}$	$\frac{2n}{1-3d}$	$\frac{(1-d)}{(1-2d)}$
Voltage stress on switch	Vo	$\frac{Vin}{(2-d)}$	$\frac{nV_{in}(1+d)}{(1-d^2)}$	$\frac{GV_{in}}{n}$ & $\frac{GV_{in}}{2n}$	$\frac{V_{in}}{(1-2d)}$
Voltage stress on Diode	Vo	$\frac{V_{in}}{(1-2d)}$	$\frac{nV_{in}(1+d)}{(1-d^2)}$	$\frac{GV_{in}}{n}$ & $\frac{GV_{in}}{2n}$	$\frac{V_{in}}{(1-2d)}$
Current stress on switch	$\frac{2I_O}{(1-d)}$	$\frac{I_O\sqrt{d}}{(2-d)}$	$\frac{2I_O}{(1-d+n)}$	$\frac{GI_o}{n}$	$\frac{I_O}{(1-2d)}$
Current stress on diode	$\frac{I_O}{(1-d)}$	$\frac{I_O}{(2-d)}$	$\frac{2I_O}{(1-d+n)}$	$\frac{GI_o}{n}$	$\frac{I_O}{(1-2d)}$
Isolation	No	No	No	Yes	No

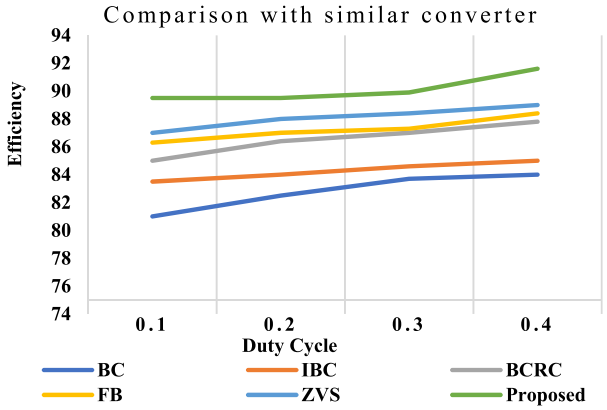

FIGURE 7. Comparison with similar converter.

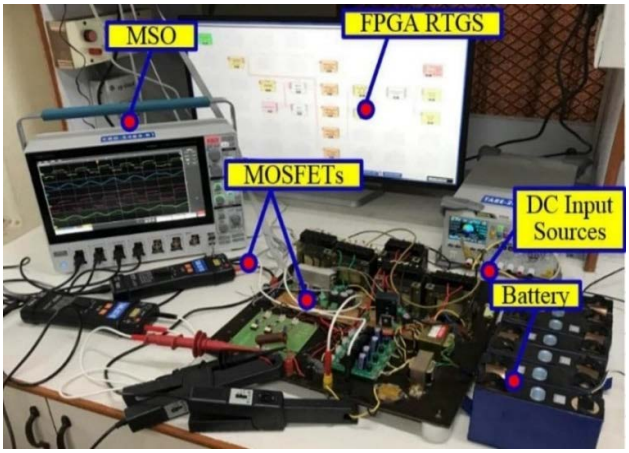

FIGURE 8. Experimental setup of proposed multiport ZQR DC/DC converter.

VI. EXPERIMENTAL RESULT

The parameter used in the simulation and experiment are tabulated in Tables 4 and 5. To validate the proposed converter's performance, a 300 W prototype version of the topology shown in Figure 8 is erected and tested in three various states.

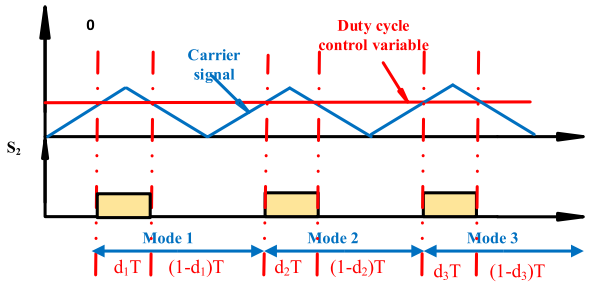

FIGURE 9. PWM generator for proposed multiport ZQRDC/DC converter.

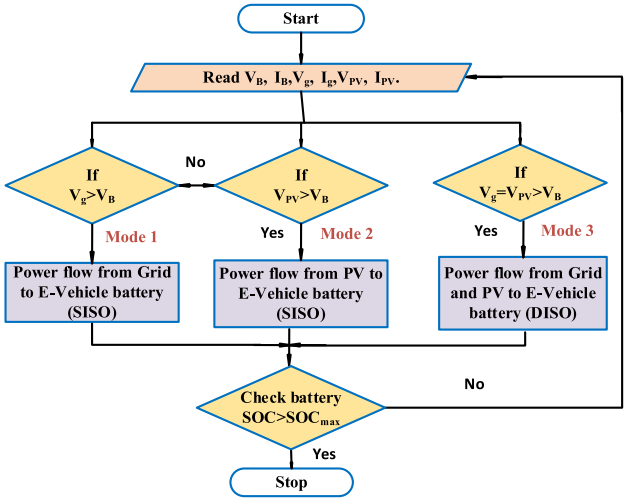

FIGURE 10. Power management strategy.

The mode of operation and the appropriate choice signals are determined by the grid power, PV power, SOC or maximum current pre-set of the battery, and the demand of load as shown in Figure 10. To maintain output voltage, a simple PWM control method [28] is used, in which an error signal is generated by comparing the output voltage to a reference voltage. The duty ratio is calculated by comparing this error to the fixed frequency carrier signal shown in Figure 9. The control signals generated by the Xilinx FPGA

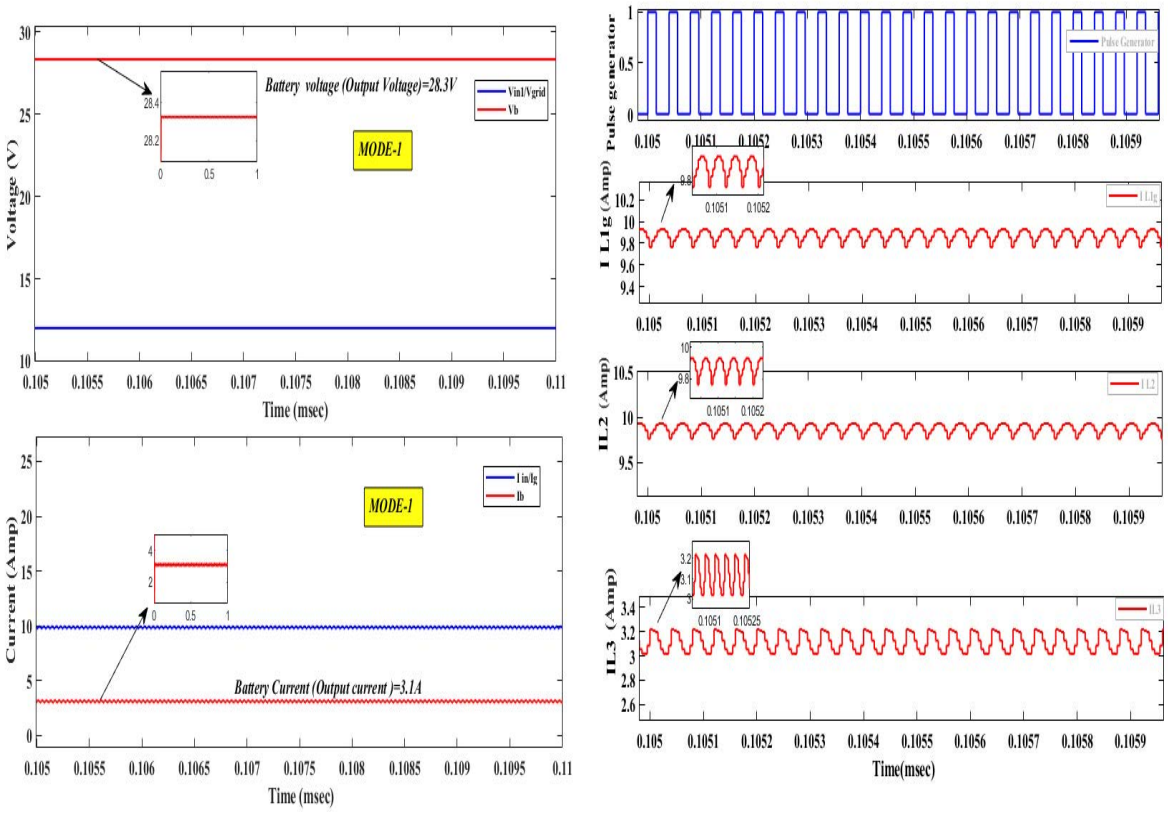

FIGURE 11. Experimental results of mode-1 (a) grid voltage,, battery voltage, grid current and battery current for duty cycle 0.4 (b) Gate pulse, inductor currents I_{L1g}, I_{L2} and I_{L3} for duty cycle 0.4.

TABLE 4. Parameters of proposed converter in simulation.

Parameter used	Simulation
Input Voltage V_{in}	12 V (Grid) for Mode 1 12 V (PV) for Mode 2 10 V (Grid) and 10 V (PV) for Mode 3
Inductors $L_{1g,} = L_{1PV} = L_2$, L_3	100 µH
Capacitor C_1 ,C_2,C_3	12.6 µF, 12.6 µF, 100 µF
Battery Rating	25.9 V,10 Ah
Switching Frequency f_s	20 KHz

TABLE 5. Parameters of proposed converter in experiment.

Parameter used	Experimental
Input Voltage V_{in}	12 V (Grid) for Mode 1, 12 V (PV) for Mode 2 10 V (Grid) and 10 V (PV) for Mode 3
Inductors $L_{1g,} = L_{1PV} = L_2$, L_3	122 µH
Capacitor C_1 ,C_2,C_3	10 µF,10 µF,100 µF
Switch S_1,S_2	IRFP4227Pbfx2 r_s=15 mΩ,C_S=46 PF
Diode D	RF1001NS2DFH r_D=20 mΩ, V_D=0.87 mV
Battery Rating	25.9 V,10 Ah
Switching Frequency f_s	20 KHz

Spartan 6 are applied to power switches as gate pulses. The gate pulses have a switching frequency of 20 kHz. As previously stated, the proposed multiport ZQR converter has the ability to charge EV battery at low duty cycle. The validation of high output gain and efficiency of multiport ZQR converter, for different duty cycles with constant input voltage is carried out.

In the proposed converter, two inputs(Grid and PV) are considered. Grid is the primary power source. and PV arrays is the secondary power source. 100 W photovoltaic (PV) panel (Mono crystalline 100 W PV panel) is used as the secondary source. Both input sources are set to 12 V. As an energy storage element, a Li-ion, 25.9 V, 10 Ah battery is used. The power management approach and strategy's flow chart is shown in Figure. 10. Li-ion batteries are widely used in EV because of their superior performance. The energy management control strategy will decide the type of input to be interfaced to the EV battery based on the availability of the inputs.

A. MODE-1 (GRID TO LOAD)

In this mode, the grid provide energy to the load (EV battery). Figure 11 and Figure 15 show the simulation and experimental results for this mode 1 operation. Grid voltage, EV battery (output) voltage, grid and battery (output) current are shown in Figure 11(a). Pulse generator and inductor current are shown in Figure 11(b).For prototype, grid voltage and current are $V_g = 12$ V and $I_g = 6.6$ A, Output battery voltage and current are $V_b = 28.3$ V and

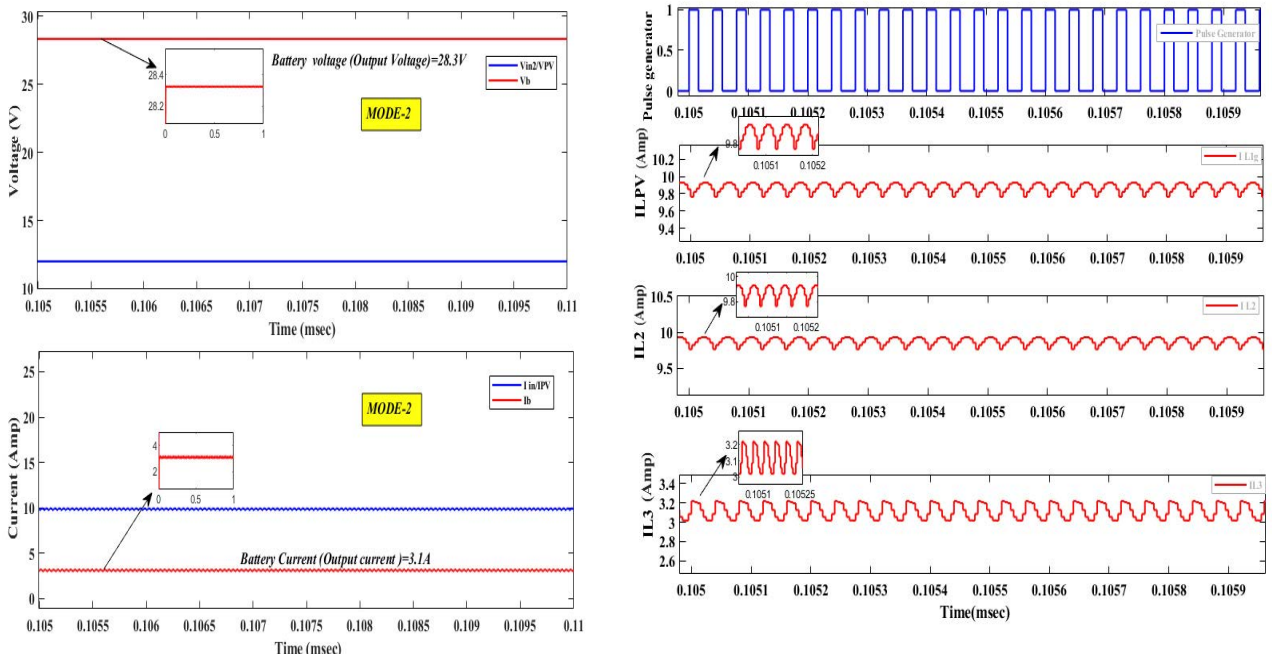

(a) (b)

FIGURE 12. Experimental results of mode-2 (a) PV voltage, battery voltage, PV current and battery current for duty cycle 0.4 (b) Gate pulse, inductor currents I_{L1g}, I_{L2} and I_{L3} for duty cycle 0.4.

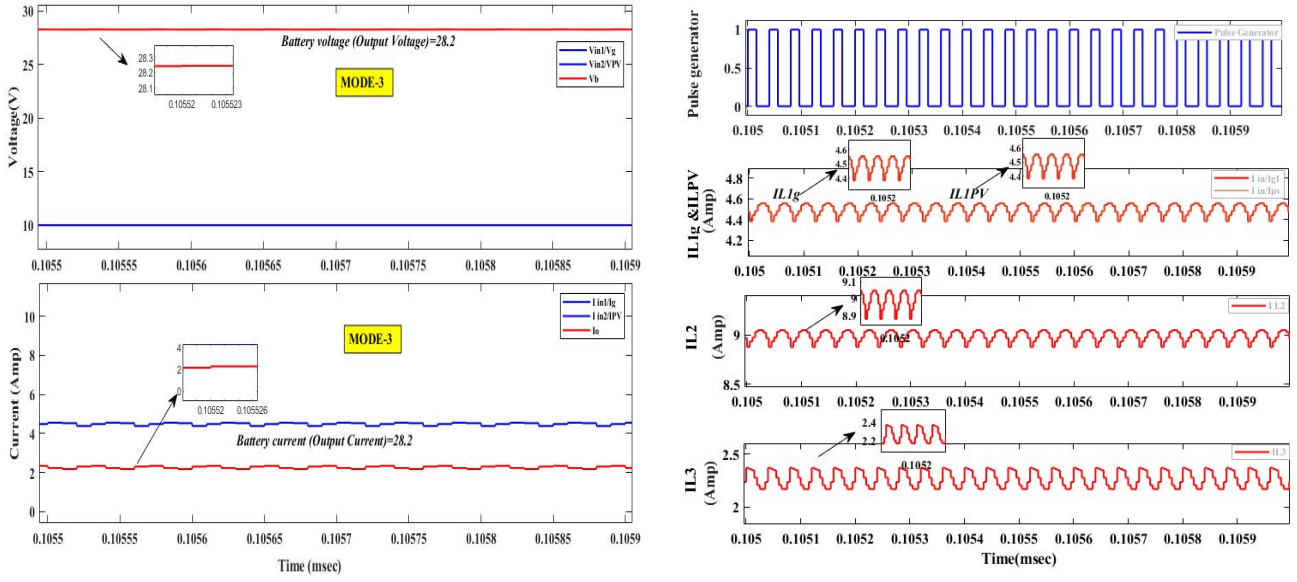

(a) (b)

FIGURE 13. Experimental results of mode-3 (a) Grid and PV voltage, battery voltage, grid and PV current and battery current for duty cycle 0.4 (b) Gate pulse, inductor currents I_{L1PV}, I_{L2} and I_{L3} for duty cycle 0.4.

$I_b = 2.9$ A at duty cycle $d_1 = 0.4$ as shown in Figure 15(a). Battery voltage is controlled by switches and the duty cycle of switch is about 0.4. The multiport ZQR- DC/DC converter is operating in boost mode. Figure 15 (b) shows the gate signal, inductor current I_{L1g}, I_{L2} and I_{L3}. The average current of inductors I_{L1gavg}, I_{L2avg}, and I_{L3avg} are 6.6 A, 6.9 A and 3.9 A respectively. Capacitor voltages C_1, C_2 are shown in Figure 15(c)

B. MODE-2 (PV TO EV BATTERY LOAD)

In this mode, the PV panel supply energy to the load (battery). Figure 12 and Figure 16 show the simulation and experimental results for this mode 2 operation. PV panel voltage, battery (output) voltage, PV panel, and EV battery (output) current are shown in Figure 12 (a). The pulse generator and inductor are shown in Figure 12 (b).Figure 16 shows the experimental results for this mode 2 operation. Grid voltage and current

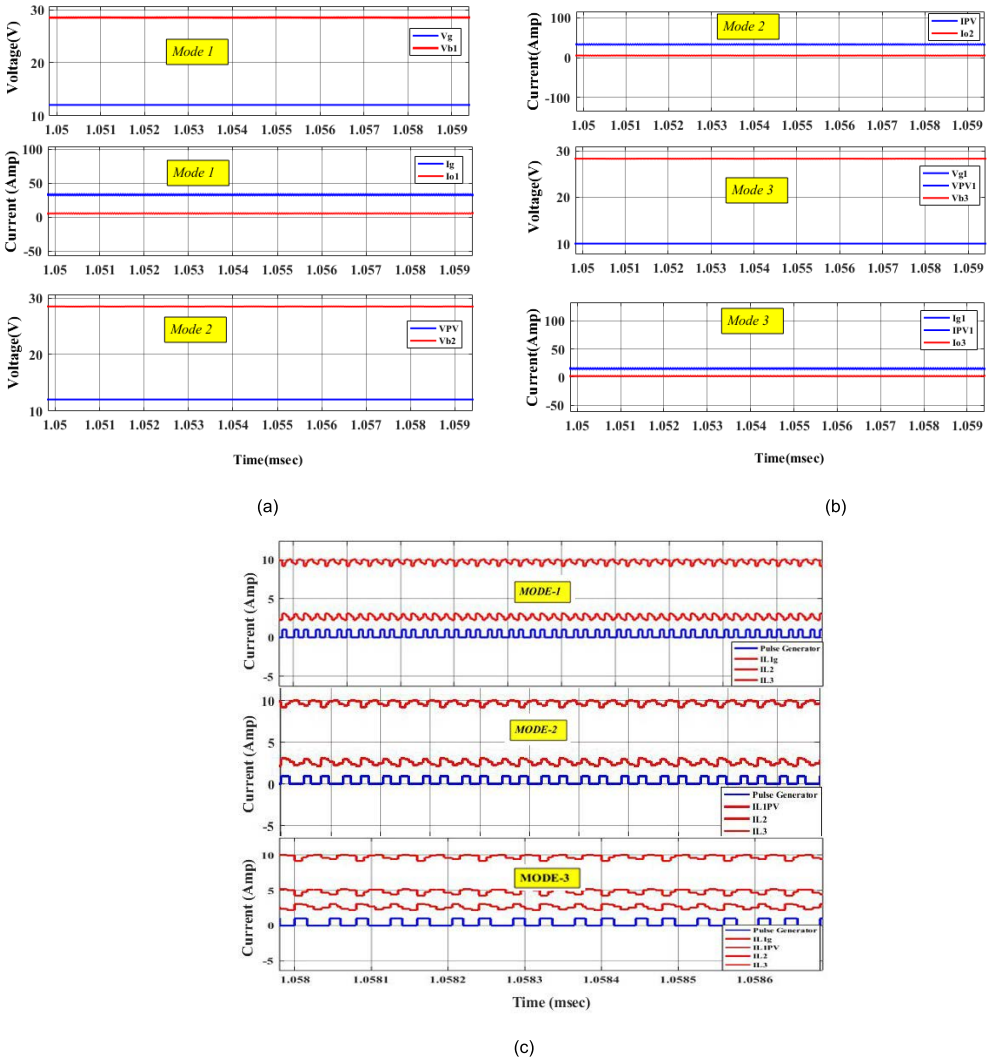

FIGURE 14. Experimental results of mode-1, mode-2 & mode-3 (a) Grid and battery voltage (mode-1), PV and battery voltage (mode-2), grid, PV and battery voltage(mode-3) for duty cycle 0.4 (b) Grid and battery current (mode-1), PV and battery current (mode-2), grid, PV and battery current (mode-3) for duty cycle 0.4 (c) Gate pulse, inductor currents I_{L1g}, I_{L1PV}, I_{L2} and I_{L3} for mode-1, mode-2 & mode-3.

TABLE 6. Comparison with similar converters.

Configuration	Components No					Specification		Expected cost
	L	*C*	*D*	HFT	*S*	Voltage Gain(dB)	Isolation	Low
Boost converter[19,20]	1	1	1	0	1	6.02	No	Moderate
Inter leaved boost converter[21]	3	3	2	0	2	6.02	No	Low
Boost converter with resonant circuit[2,22]	3	3	5	0	2	5.42	No	Moderate
Full bridge boost converter[23]	1	2	4	1	4	6.02	Yes	Moderate
Isolated ZVS converter[2,5]	1	3	7	1	6	3.52	Yes	High
Proposed converter (Z-QRC)	4	3	1	0	2	9.54	No	Moderate

Table representation: L- inductor, C -capacitor, D -diode, HFT -High frequency transformer, S Switch

are $V_{PV} = 12$ V and $I_{PV} = 6.9$ A, Output battery voltage and current $V_b = 25.8$ V and $I_b = 2.4$ A at duty cycle $d_2 = 0.4$ are shown in Figure 16 (a). EV battery voltage is controlled by switch. The Figure 16 (b) shows the gate signal, current of inductors are I_{L1g}, I_{L2} and I_{L3}. The average current of inductors $I_{L1pvavg}$, I_{L2avg}, and I_{L3avg} are 6.8 A,7 A and 3.8 A respectively. capacitor voltage C_1, C_2 are shown in Figure 16 (C).

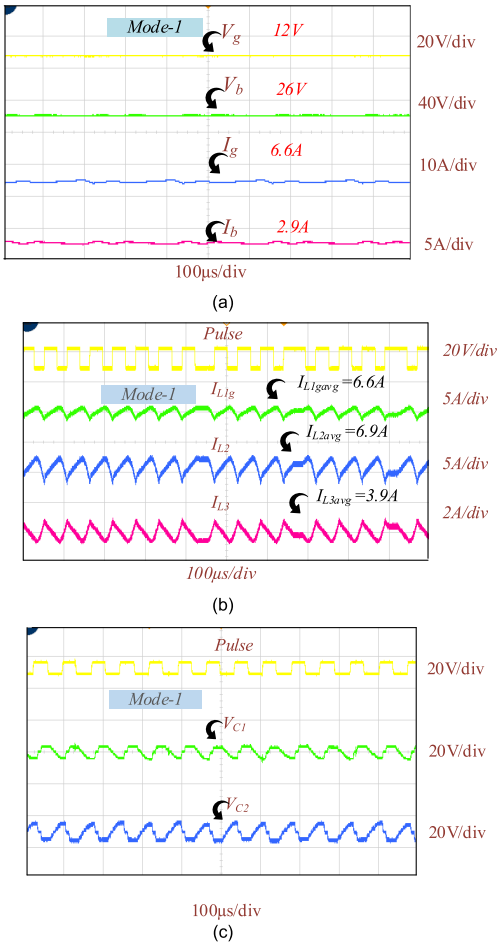

FIGURE 15. Experimental results of mode-1 (a) Grid voltage, EV battery voltage, grid current, and battery current for duty cycle 0.4 (b) Gate pulse, Inductor currents I_{L1g}, I_{L2} and I_{L3} (top to bottom) for duty cycle 0.4 (c) Gate pulse, capacitor voltage V_{C1} and V_{C2} (top to bottom) for duty cycle 0.4.

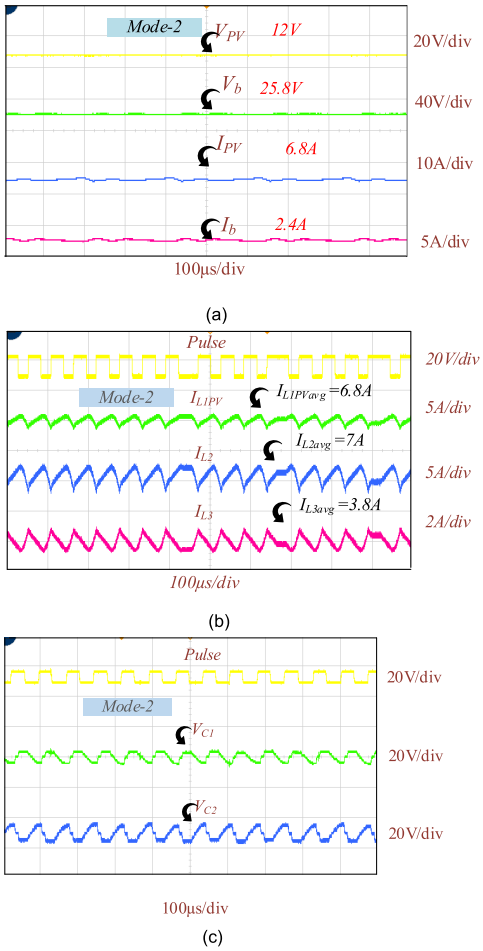

FIGURE 16. Experimental results of mode-2 (a) PV voltage, EV battery voltage, PV current and battery current for duty cycle 0.4 (b) Gate pulse, Inductor currents I_{L1PV}, I_{L2} and I_{L3} (top to bottom) for duty cycle 0.4 (c) Gate pulse, capacitor voltage V_{C1} and V_{C2} (top to bottom) for duty cycle 0.4.

C. MODE-3 (GRID & PV TO EV BATTERY LOAD)

In this mode, both grid and PV panel provide energy to the load (EV battery). Figure 13 and Figure 17 show the simulation and experimental results for this mode 3 operation. Grid voltage, PV panel voltage, EV battery (output) voltage, grid, PV panel, and EV battery (output) current are shown in Figure 13 (a). The pulse generator and inductor are shown in Figure 13 (b).

Figure 17 shows the experimental results for this mode 2 operation. Primary source grid voltage and current are V_g = 10 V and I_g = 5.3 A, secondary source PV voltage and current are V_{PV} = 10 V and I_{PV} = 5.1 A Output battery voltage and current are V_b = 28 V and I_b = 3.1 A at duty cycle $d_3 = 0.4$ as shown in Figure 17 (a), (b) and (c). Battery Voltage is controlled by duty cycle. Figure 17 (d) shows the gate signal, inductor current I_{L1g}, I_{L2} and I_{L3}. The average current of inductors I_{L1gavg}, $I_{L1pvavg}$, I_{L2avg}, and I_{L3avg} are 4.8 A, 4.9 A, 4.9 A and 5.2 A respectively. capacitor voltage C_1, C_2 are shown in Figure 17 (e).

When designing a charging system for EVs, the cost of DC/DC converters is a significant aspect to consider. To anticipate a comparable cost, the quantity of switches, transformers, capacitors, diodes, and inductors utilised in various DC/DC converters must be reduced. Experimental output results of all the three modes shown in Figure 14 Table 6 presents the simple component and voltage gain comparison of converter topologies discussed in this paper

VII. DYNAMIC ANALYSIS FOR THE PROPOSED CONVERTER

In order to assess the dynamic behaviour of the proposed multiport ZQR DC/DC converter the input voltage variation is shown in Figure (18-20). The suggested multiport ZQR DC/DC converter has an obvious rapid transient performance for an open loop system. The proposed Multi ZQR DC/DC converter is simulated in MATLAB-Simulink platform for open loop.

A. CASE 1 (VARIATION IN GRID VOLTAGE)

Under steady-state condition, the grid voltage is varied from 67% to 80% of supply voltage (15 V) (i.e 10 V

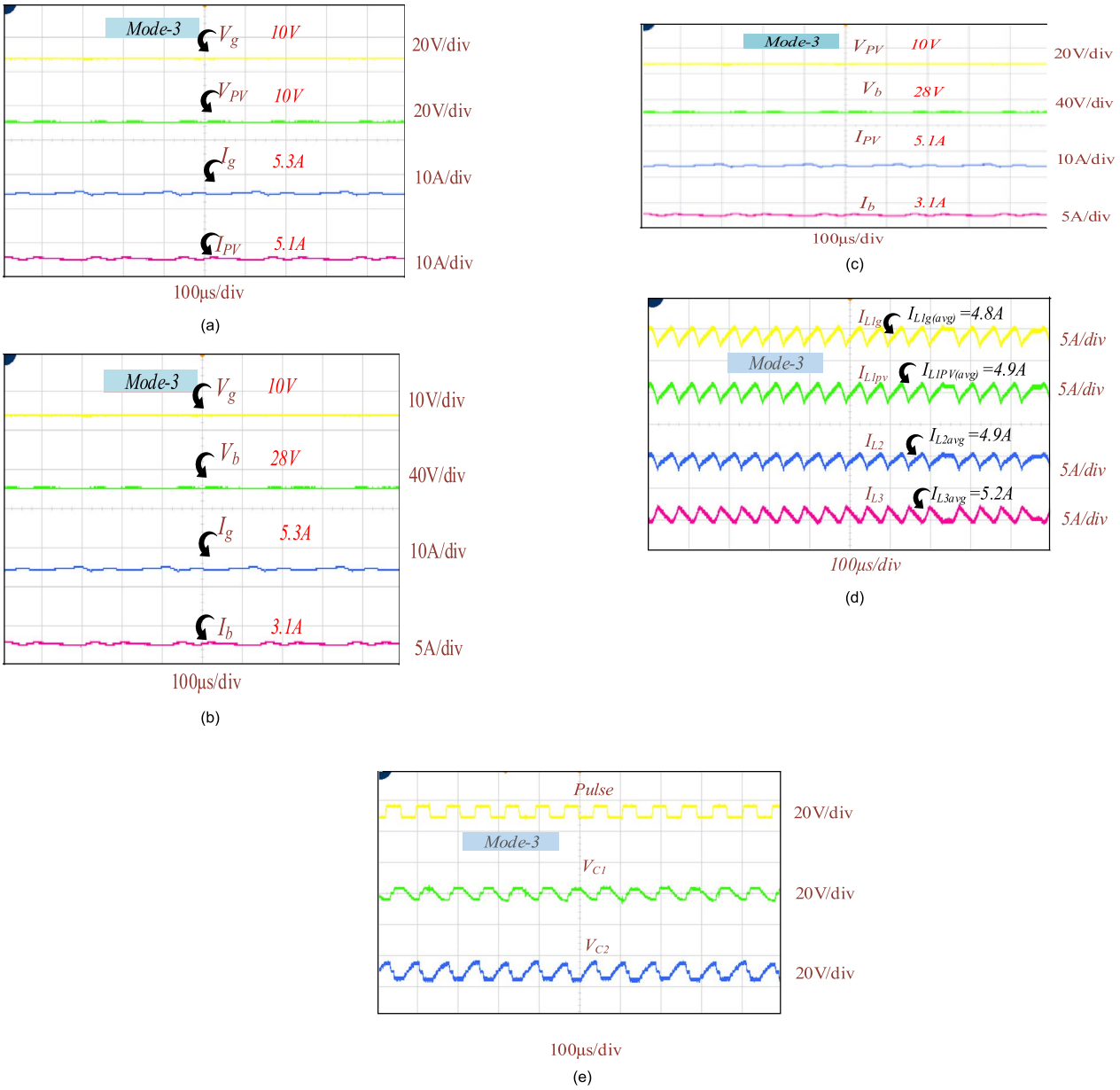

FIGURE 17. Experimental results of mode-3 (a) Grid & PV voltage, grid & PV current, load voltage and load current for duty cycle 0.4 (b) grid & EV battery voltage, grid & EV battery current for duty cycle 0.4 (c) PV & EV battery voltage, PV & battery current for duty cycle 0.4 (d) Gate pulse, inductor currents I_{L1g}, I_{L1PV}, I_{L2} and I_{L3} (top to bottom) for duty cycle 0.4 (e) Gate pulse, V_{C1} and V_{C2} (top to bottom) for duty cycle 0.4.

to 12 V), and the grid current is varied from 8.9 A to 10 A as shown in Figure 18. It can be seen that the output voltage and current increase from 27.8 V to 28.2 V and 2.9 A to 5.75 A, due to variation in grid voltage.

B. CASE 2 (VARIATION IN PV VOLTAGE)

In this case, during the steady-state condition, when PV voltage is varied from 67% to 80% of net voltage (15 V) grid current vary from 8.8 A to 10.1 A as shown in Figure 19. It can be seen that the output voltage and current increase from 27.8 V to 28.3 V and 2.8 A to 5.8 A, due to variation in PV voltage.

C. CASE 3 (VARIATION IN BOTH GRID AND PV VOLTAGE)

In case 3 the grid and PV voltage are varied from 67% to 100% of supply voltage (15 V) (i.e 10 V to 15 V), grid and PV current are varied from 8.9 A to 12.2 A as shown in Figure 20. It can be seen that the output voltage and current increase from 27.8 V to 28.1 V and 2.8 A to 5.6 A, due to variation in grid and PV voltage.

From the simulation and experimental observation of multiport ZQR DC/DC converter for off board EV battery charging, it can be understood that the voltage gain & the efficiency of the proposed converter increase at lower duty cycles. Also, it is worth mentioning that, as seen from the

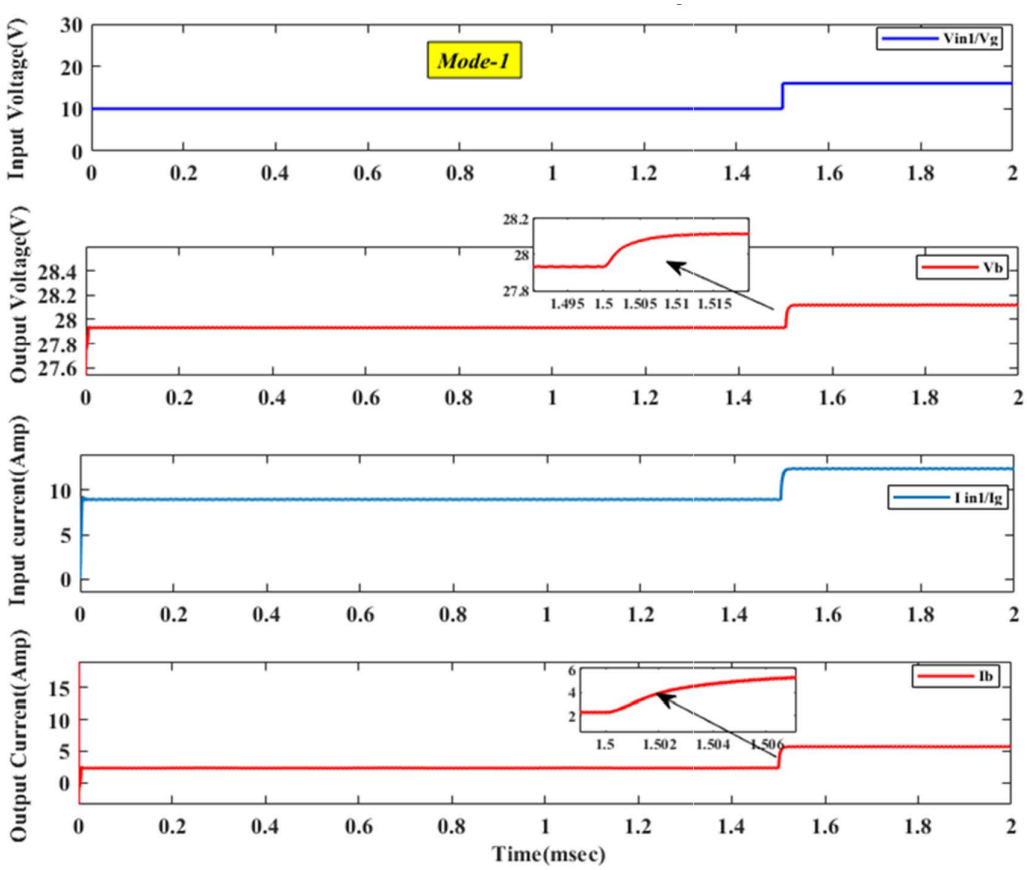

FIGURE 18. Dynamic analysis of the proposed converter in mode-1: Grid voltage, EV Battery voltage, grid current and battery current for duty cycle 0.4.

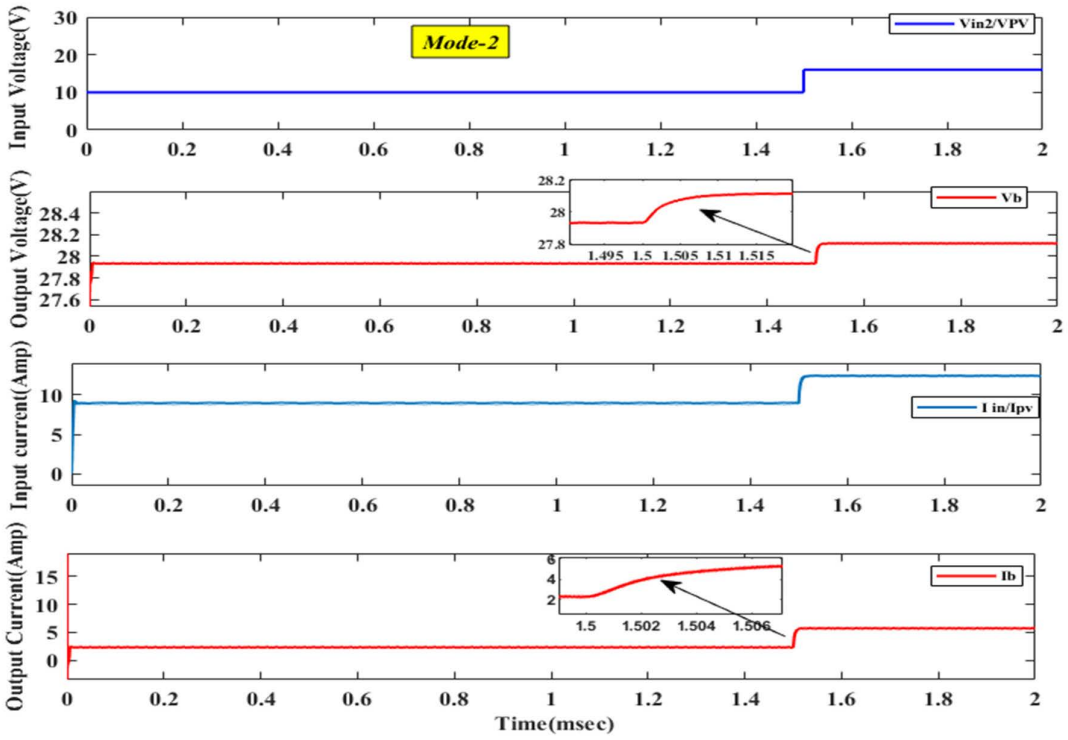

FIGURE 19. Dynamic analysis of the proposed converter in mode-2 -PV voltage, battery voltage, PV current and battery current for duty cycle 0.4.

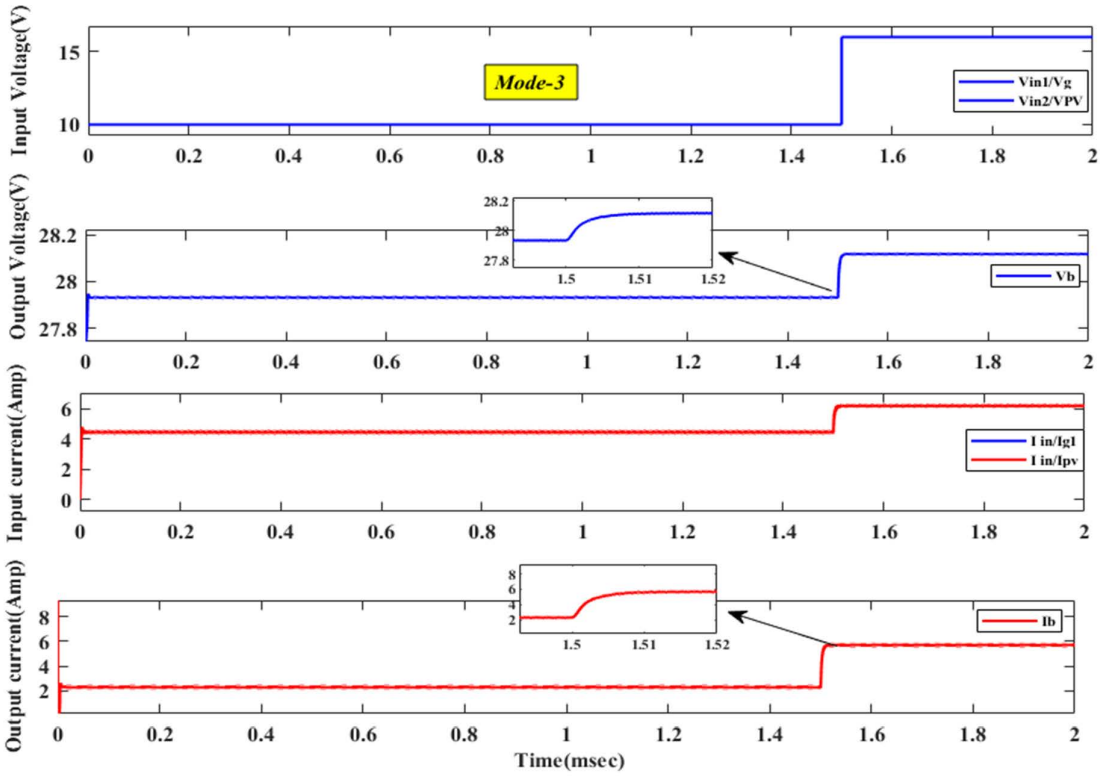

FIGURE 20. Dynamic analysis of the proposed converter in mode-3 - Grid voltage, PV voltage, EV battery voltage, grid current, PV current and battery current for duty cycle 0.4.

derived performance equations, the proposed multiport ZQR DC/DC converter has a desirable efficiency.

VIII. CONCLUSION

In this paper, a modified multiport ZQR DC/DC converter for off board EV battery charging was proposed. The proposed converter has the advantages of improved step-up ratio, reduced switch voltage stress, continuous current even at 0.4 duty cycle. The converter has the feature of power sharing between the input ports and supplying steady power to EV battery even in the absence of any one source. The demonstrated experimental results prove the principle of operation and validate the presented theoretical and simulation analyses in terms of steady state, dynamic and loss analyses. Though the comparison of proposed multiport ZQR DC/DC converter with conventional converters proves the efficacy of the designed converter, it has its own limitation of restricting the gain to three times with a single resonant buffer unit. The abovesaid limitation can be overcome with the inclusion of additional buffer units in parallel. Finally, the results presented to verify the design procedure, and performance of the converter topology confirm the suggested topology as a viable solution for EV off board charging.

This paper has elaborated the design principle and work of three port ZQR DC/DC converter for EV off board charging. The research work can be extended with

(i) the analysis of high gain ZQR DC/DC converter with multiple EVs and

(ii) developing the optimized control strategy for controlling the battery charging and discharging of EV batteries in a MIMO EV charging system.

REFERENCES

[1] F. Guo, L. Fu, X. Zhang, C. Yao, H. Li, and J. Wang, "A family of quasi-switched-capacitor circuit-based dual-input DC/DC converters for photovoltaic systems integrated with battery energy storage," *IEEE Trans. Power Electron.*, vol. 31, no. 12, pp. 8237–8246, Dec. 2016, doi: 10.1109/TPEL.2016.2519394.

[2] S. Chakraborty, H.-N. Vu, M. M. Hasan, D.-D. Tran, M. E. Baghdadi, and O. Hegazy, "DC-DC converter topologies for electric vehicles, plug-in hybrid electric vehicles and fast charging stations: State of the art and future trends," *Energies*, vol. 12, no. 8, p. 1569, Apr. 2019, doi: 10.3390/en12081569.

[3] S. Habib, M. M. Khan, F. Abbas, A. Ali, M. T. Faiz, F. Ehsan, and H. Tang, "Contemporary trends in power electronics converters for charging solutions of electric vehicles," *CSEE J. Power Energy Syst.*, vol. 6, no. 4, pp. 911–929, Dec. 2020, doi: 10.17775/CSEEJPES.2019.02700.

[4] C. Yao, X. Ruan, X. Wang, and C. K. Tse, "Isolated buck–boost DC/DC converters suitable for wide input-voltage range," *IEEE Trans. Power Electron.*, vol. 26, no. 9, pp. 2599–2613, Sep. 2011, doi: 10.1109/TPEL.2011.2112672.

[5] F. A. A. Meinagh, E. Babaei, H. Tarzamni, and P. Kolahian, "Isolated high step-up switched-boost DC/DC converter with modified control method," *IET Power Electron.*, vol. 12, no. 14, pp. 3635–3645, Nov. 2019, doi: 10.1049/iet-pel.2018.6114.

[6] M. A. Salvador, T. B. Lazzarin, and R. F. Coelho, "High step-up DC–DC converter with active switched-inductor and passive switched-capacitor networks," *IEEE Trans. Ind. Electron.*, vol. 65, no. 7, pp. 5644–5654, Jul. 2018, doi: 10.1109/TIE.2017.2782239.

[7] C.-C. Lin, L.-S. Yang, and G. W. Wu, "Study of a non-isolated bidirectional DC-DC converter," *IET Power Electron.*, vol. 6, no. 1, pp. 30–37, Jan. 2013, doi: 10.1049/iet-pel.2012.0338.

[8] S.-J. Jeon and G.-H. Cho, "A zero-voltage and zero-current switching full bridge DC–DC converter with transformer isolation," *IEEE Trans. Power Electron.*, vol. 16, no. 5, pp. 573–580, Sep. 2001.
[9] D. Bao, A. Kumar, X. Pan, X. Xiong, A. R. Beig, and S. K. Singh, "Switched inductor double switch high gain DC-DC converter for renewable applications," *IEEE Access*, vol. 9, pp. 14259–14270, 2021, doi: 10.1109/ACCESS.2021.3051472.
[10] V. Karthikeyan, K. Sundaramoorthy, G. Guru Kumar, and E. Babaei, "Regenerative switched-inductor/capacitor type DC–DC converter with large voltage gain for PV applications," *IET Power Electron.*, vol. 13, no. 1, pp. 68–77, Jan. 2020, doi: 10.1049/iet-pel.2019.0408.
[11] A. Kawa, R. Stala, A. Mondzik, S. Pirog, and A. Penczek, "High-power thyristor-based DC–DC switched-capacitor voltage multipliers: Basic concept and novel derived topology with reduced number of switches," *IEEE Trans. Power Electron.*, vol. 31, no. 10, pp. 6797–6813, Oct. 2016, doi: 10.1109/TPEL.2015.2505906.
[12] J. Yang, Z. He, H. Pang, and G. Tang, "The hybrid-cascaded DC–DC converters suitable for HVdc applications," *IEEE Trans. Power Electron.*, vol. 30, no. 10, pp. 5358–5363, Oct. 2015, doi: 10.1109/TPEL.2015.2420666.
[13] N. K. Shereef, N. Mani, and N. John, "A novel DC–DC boost converter based on voltage-lift technique," *Int. J. Innov. Eng. Technol.*, vol. 11, no. 3, pp. 61–68, 2018.
[14] F. A. A. Meinagh, E. Babaei, and H. Tarzamni, "Modified high voltage gain switched boost inverter," *IET Power Electron.*, vol. 10, no. 13, pp. 1655–1664, Oct. 2017, doi: 10.1049/iet-pel.2016.0597.
[15] A. M. S. S. Andrade, E. Mattos, L. Schuch, H. L. Hey, and M. L. da Silva Martins, "Synthesis and comparative analysis of very high step-up DC–DC converters adopting coupled-inductor and voltage multiplier cells," *IEEE Trans. Power Electron.*, vol. 33, no. 7, pp. 5880–5897, Jul. 2018, doi: 10.1109/TPEL.2017.2742900.
[16] A. Mirzaei, A. Jusoh, Z. Salam, E. Adib, and H. Farzanehfard, "Analysis and design of a high efficiency bidirectional DC–DC converter for battery and ultracapacitor applications," *Simul. Model. Pract. Theory*, vol. 19, no. 7, pp. 1651–1667, Aug. 2011, doi: 10.1016/j.simpat.2011.04.007.
[17] M. Forouzesh, Y. Shen, K. Yari, Y. P. Siwakoti, and F. Blaabjerg, "High-efficiency high step-up DC–DC converter with dual coupled inductors for grid-connected photovoltaic systems," *IEEE Trans. Power Electron.*, vol. 33, no. 7, pp. 5967–5982, Jul. 2018, doi: 10.1109/TPEL.2017.2746750.
[18] Y. P. Siwakoti and F. Blaabjerg, "Single switch nonisolated ultra-step-up DC–DC converter with an integrated coupled inductor for high boost applications," *IEEE Trans. Power Electron.*, vol. 32, no. 11, pp. 8544–8558, Nov. 2017, doi: 10.1109/TPEL.2016.2646382.
[19] M. Forouzesh, P. Y. Siwakoti, A. S. Gorji, F. Blaabjerg, and B. Lehman, "Step-up DC–DC Converters: A comprehensive review of voltage-boosting techniques, topologies, and applications," *IEEE Trans. Power Electron.*, vol. 32, no. 12, pp. 9143–9178, Dec. 2017, doi: 10.1109/TPEL.2017.2652318.
[20] K. Suresh, C. Bharatiraja, N. Chellammal, M. Tariq, R. K. Chakrabortty, M. J. Ryan, and B. Alamri, "A multifunctional non-isolated dual input-dual output converter for electric vehicle applications," *IEEE Access*, vol. 9, pp. 64445–64460, 2021, doi: 10.1109/ACCESS.2021.3074581.
[21] M. Esteki, B. Poorali, E. Adib, and H. Farzanehfard, "Interleaved buck converter with continuous input current, extremely low output current ripple, low switching losses, and improved step-down conversion ratio," *IEEE Trans. Ind. Electron.*, vol. 62, no. 8, pp. 4769–4776, Aug. 2015, doi: 10.1109/TIE.2015.2397881.
[22] T.-F. Wu, Y.-S. Lai, J.-C. Hung, and Y.-M. Chen, "Boost converter with coupled inductors and buck–boost type of active clamp," *IEEE Trans. Ind. Electron.*, vol. 55, no. 1, pp. 154–162, Jan. 2008, doi: 10.1109/TIE.2007.903925.
[23] J. Saeed and A. Hasan, "Control-oriented discrete-time large-signal model of phase-shift full-bridge DC–DC converter," *Electr. Eng.*, vol. 100, no. 3, pp. 1431–1439, Sep. 2018, doi: 10.1007/s00202-017-0601-8.
[24] M. Brenna, F. Foiadelli, C. Leone, and M. Longo, "Electric vehicles charging technology review and optimal size estimation," *J. Electr. Eng. Technol.*, vol. 15, no. 6, pp. 2539–2552, Nov. 2020, doi: 10.1007/s42835-020-00547-x.
[25] W. Su, H. Rahimi-Eichi, W. Zeng, and M. Chow, "Smart grid environment," *IEEE Trans. Ind. Informat.*, vol. 8, no. 1, pp. 1–10, Feb. 2012.
[26] A. Dubey and S. Santoso, "Electric vehicle charging on residential distribution systems: Impacts and mitigations," *IEEE Access*, vol. 3, pp. 1871–1893, 2015, doi: 10.1109/ACCESS.2015.2476996.
[27] T. Kayiranga, H. Li, X. Lin, Y. Shi, and H. Li, "Abnormal operation state analysis and control of asymmetric impedance network-based quasi-Z-source PV inverter (AIN-qZSI)," *IEEE Trans. Power Electron.*, vol. 31, no. 11, pp. 7642–7650, Nov. 2016, doi: 10.1109/TPEL.2016.2515995.
[28] F. Z. Peng, "Z-source inverter," *IEEE Trans. Ind. Appl.*, vol. 39, no. 2, pp. 504–510, Mar./Apr. 2003.
[29] J. W. Yang and S. K. Han, "A Si-FET-based high switching frequency three-level LLC resonant converter," *Energies*, vol. 12, no. 16, p. 3082, Aug. 2019, doi: 10.3390/en12163082.
[30] Y. Zhang, C. Fu, M. Sumner, and P. Wang, "A wide input-voltage range quasi-Z-source boost DC–DC converter with high-voltage gain for fuel cell vehicles," *IEEE Trans. Ind. Electron.*, vol. 65, no. 6, pp. 5201–5212, Jun. 2018, doi: 10.1109/TIE.2017.2745449.
[31] B. Pooralii, H. M. Jazi, and E. Adib, "Improved high step-up Z-source DC–DC converter with single core and ZVT operation," *IEEE Trans. Power Electron.*, vol. 33, no. 11, pp. 9647–9655, Nov. 2018.
[32] F. A. A. Meinagh, J. Yuan, and Y. Yang, "Analysis and design of a high voltage-gain quasi-Z-source DC–DC converter," *IET Power Electron.*, vol. 13, no. 9, pp. 1837–1847, Jul. 2020, doi: 10.1049/iet-pel.2019.1165.
[33] S. Khosrogorji, M. Ahmadian, H. Torkaman, and S. Soori, "Multi-input DC/DC converters in connection with distributed generation units—A review," *Renew. Sustain. Energy Rev.*, vol. 66, pp. 360–379, Dec. 2016, doi: 10.1016/j.rser.2016.07.023.
[34] H. Wu, J. Zhang, and Y. Xing, "A family of multiport buck–boost converters based on DC-link-inductors (DLIs)," *IEEE Trans. Power Electron.*, vol. 30, no. 2, pp. 735–746, Feb. 2015.
[35] B. Chandrasekar, C. Nallaperumal, S. Padmanaban, M. S. Bhaskar, J. B. Holm-Nielsen, Z. Leonowicz, and S. O. Masebinu, "Non-isolated high-gain triple port DC–DC buck-boost converter with positive output voltage for photovoltaic applications," *IEEE Access*, vol. 8, pp. 113649–113666, 2020, doi: 10.1109/ACCESS.2020.3003192.

S. HARINI received the B.E. degree from Avinashilingam University, India, in 2010, and the M.E. degree in power electronics and drives from Anna University, in 2014. She is currently pursuing the Ph.D. degree with the SRM Institute of Science and Technology, India, with a focus on design of power electronic converters for electric vehicle applications. Her research interests include design and control of power electronic converters and renewable energy systems.

N. CHELLAMMAL (Member, IEEE) received her M.S. degree in Electrical Drives and Automation from Tashkent State Technical University, Tashkent, CIS (a former USSR) and her Ph.D. degree in Power Electronics from the Faculty of Engineering, SRM Institute of Science and Technology, Chennai, India. She is currently working as an Associate Professor at the SRM Institute of Science and Technology. She has authored or co-authored more than 30 papers which are published in international journal including IEEE Access, Wiley and IEEE international conferences etc. She is also serving as reviewer for many peer reviewed journals including IEEE Transactions. Her research interests include modelling of power electronic converters and drives, EV charging, grid integration of renewable energy resources and design of controllers.

BHARATIRAJA CHOKKALINGAM (Senior Member, IEEE) received the Bachelor of Engineering degree in electrical and electronics engineering from the Kumaraguru College of Engineering, Coimbatore, India, in 2002, the Master of Engineering degree in power electronics engineering from the Government College of Technology, Coimbatore, in 2006, and the Ph.D. degree, in 2015.

He completed his first Postdoctoral Fellowship at the Centre for Energy and Electric Power, Faculty of Engineering and the Built Environment, Tshwane University of Technology, South Africa, in 2016, with the National Research Foundation funding. He is currently working as an Associate Professor at the Department of Electrical and Electronics Engineering, SRM Institute of Science and Technology, Kattankulathur Campus, Chennai, India. He is also a Visiting Researcher Scientist at Northeastern University, Boston, USA. He is also a Visiting Researcher at the University of South Africa. He has authored more than 110 research papers, which are published in international journals, including various IEEE TRANSACTIONS. His research interests include power electronics converter topologies, controls for PV and EV applications, PWM techniques for power converters and adjustable speed drives, wireless power transfer, and smart grid. He is a Senior Member of IEI and IET. He was the Award recipient of DST; Indo-U.S. Bhaskara Advanced Solar Energy, in 2017, and through he completed his second Postdoctoral Fellowship at the Department of Electrical and Computer Engineering, Northeastern University, USA. He is also an Award recipient of Young Scientists Fellowship, Tamil Nadu State Council for Science and Technology, in 2018. He is also an Award recipient of Young Scientists Fellowship, Tamil Nadu State Council for Science and Technology, in 2018. He was collaborated with leading Indian overseas universities for both teaching and research. He has completed six sponsored projects from various government and private agencies. He also singed MoU with various industries. Currently, he is running two funded research project in wireless charging of EV and UAV under DST SERB Core Research Grant, Government of India.

LUCIAN MIHET-POPA (Senior Member, IEEE) was born in 1969. He received the bachelor's degree in electrical engineering, the master's degree in electric drives and power electronics, and the Ph.D. and Habilitation degrees in electrical engineering from the Politehnica University of Timisoara, Romania, in 1999, 2000, 2002, and 2015, respectively. Since 2016, he has been working as a Full Professor in energy technology with the Østfold University College, Norway. From 1999 to 2016, he was with the Politehnica University of Timisoara. He has also worked as a Research Scientist with Danish Technical University, from 2011 to 2014, and also with Aalborg University, Denmark, from 2000 to 2002. He held a postdoctoral position with Siegen University, Germany, in 2004. He is also the Head of the Research Laboratory ''Intelligent Control of Energy Conversion and Storage Systems'' and is one of the Coordinators of the master's degree program in ''Green Energy Technology'' with the Faculty of Engineering, Østfold University College. He has published more than 130 papers in national and international journals and conference proceedings and ten books. He has served as a scientific and a technical program committee member for many IEEE conferences. He has participated in more than 15 international grants/projects, such as FP7, EEA, and Horizon 2020. He has been awarded more than ten national research grants. His research interests include modeling, simulation, control, testing of energy conversion systems, and distributed energy resources (DER) components and systems, including battery storage systems (BSS) [for electric vehicles and hybrid cars and vanadium redox batteries (VRB)] and energy efficiency in smart buildings and smart grids. He was invited to join the Energy and Automotive Committees by the President and the Honorary President of the Atomium European Institute, working in close cooperation with—under the umbrella—the EC and EU Parliament, and was also appointed as the Chairperson of AI4People, Energy Section. Since 2017, he has been a Guest Editor of five special issues of *Energies* (MDPI), *Applied Sciences*, *Majlesi Journal of Electrical Engineering*, and *Advances in Meteorology* journals.